Length-Dependent Thermopower of Highly Conducting Au−C Bonded Single Molecule Junctions

J. R. Widawsky,[†] W. Chen,[§] H. Vázquez,[†] T. Kim,[†,§] R. Breslow,[§] M. S. Hybertsen,[‡] and L. Venkataraman*,[†]

[†]Department of Applied Physics and Applied Mathematics, Columbia University, New York, New York, United States
[‡]Center For Functional Nanomaterials, Brookhaven National Laboratory, Upton, New York, United States
[§]Department of Chemistry, Columbia University, New York, New York, United States

Ⓢ Supporting Information

ABSTRACT: We report the simultaneous measurement of conductance and thermopower of highly conducting single-molecule junctions using a scanning tunneling microscope-based break-junction setup. We start with molecular backbones (alkanes and oligophenyls) terminated with trimethyltin end groups that cleave off in situ to create junctions where terminal carbons are covalently bonded to the Au electrodes. We apply a thermal gradient across these junctions and measure their conductance and thermopower. Because of the electronic properties of the highly conducting Au−C links, the thermoelectric properties and power factor are very high. Our results show that the molecular thermopower increases nonlinearly with the molecular length while conductance decreases exponentially with increasing molecular length. Density functional theory calculations show that a gateway state representing the Au−C covalent bond plays a key role in the conductance. With this as input, we analyze a series of simplified models and show that a tight-binding model that explicitly includes the gateway states and the molecular backbone states accurately captures the experimentally measured conductance and thermopower trends.

KEYWORDS: Molecular thermopower, molecular conductance, density functional theory, Au−C covalent bonds
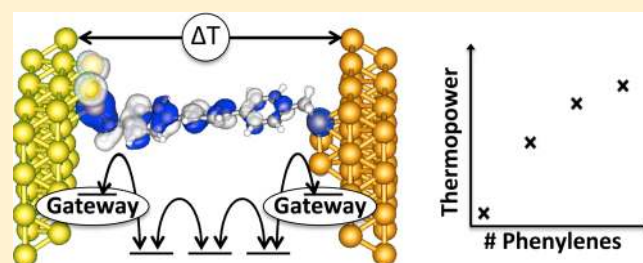
The development of viable thermoelectric devices using organic-based materials has centered around finding materials that maximize the thermoelectric figure of merit,[1,2] $ZT = GS^2T/\kappa$, where G is the electrical conductance, S is the thermopower, and κ is the thermal conductivity. Measuring material performance on a fundamental length scale at the single-molecule level[3] can thus provide a better understanding of structure−function relations in these systems. Reliable thermoelectric measurements of molecular assemblies with metal electrodes[4−6] and at the single-molecule level[7−11] have recently been carried out with different organic systems. In this work, we measure conductance and thermopower for a series of trimethyl-tin-terminated oligophenyls and alkanes that bind directly to Au electrodes by forming covalent Au−C sigma bonds[12] after the trimethyl-tin groups cleave in situ. The conductances of the oligophenyls range from about 0.9 G_0 for a single benzene to 1.0×10^{-3} G_0 for tetraphenyl,[12] the longest in this series, and our results show that we maximize the power factor, GS^2, for the biphenyl (which has a conductance of about 0.1 G_0 and a thermopower of 14.3 μV/K) at 1.6 fW/K². We also measure conductance and thermopower for alkanes with 6 to 10 methylene units that bind through Au−C bonds. Their conductance ranges from 1.4×10^{-2} to 2.5×10^{-4} G_0 and show thermopowers of 5.0−5.6 μV/K. This is significantly larger than

what we have measured for phosphine-linked alkane chains,[8] indicating that these alkane based molecular junctions can have a substantial thermopower despite their low conductance. To explain these results, we examine density functional theory based calculations of electron transmission through exemplary model structures for these junctions. The results indicate that gateway states representing Au−C sigma bonds at the links play a key role. In contrast to more simplified models, a tight-binding model that explicitly includes these gateway states in addition to molecular backbone states accurately captures the experimentally measured trends in conductance and thermopower and reproduces the essential qualitative features from the density functional theory based calculations.

In a single-molecule junction, the thermopower or Seebeck coefficient, S, determines the magnitude of the built-in potential developed across a material (or molecular junction) when a temperature difference, ΔT, is applied. With the additional presence of an external voltage bias, ΔV, across the junction,[13,14] the total current, I, is simply given by $I = -G\Delta V + GS\Delta T$, where G is the electrical conductance. The

thermopower can be measured either from the zero-bias thermoelectric current ($S = I/G\Delta T$ when $\Delta V = 0$) or from the open circuit voltage ($S = \Delta V/\Delta T$ when $I = 0$). These equations apply to both bulk materials, where transport is, for example, diffusive[15] and to single-molecule junctions, where transport can be coherent.[13] For coherent tunneling, the conductance through a molecular junction in the zero-bias limit is given by the Landauer formula,[13,15] $G = [(2e^2)/h]\mathcal{T}(E_F)$, and the thermopower becomes

$$S = -\frac{\pi^2 k_B^2 T}{3e\mathcal{T}(E)}\frac{\partial \mathcal{T}(E)}{\partial E}\bigg|_{E=E_F}$$

We simultaneously measure the conductance and thermopower of single-molecule junctions using the scanning tunneling microscope-based break junction technique[16,17] (STM-BJ). A schematic of the circuitry as well as the STM layout is shown in Figure 1a. Single-molecule junctions are
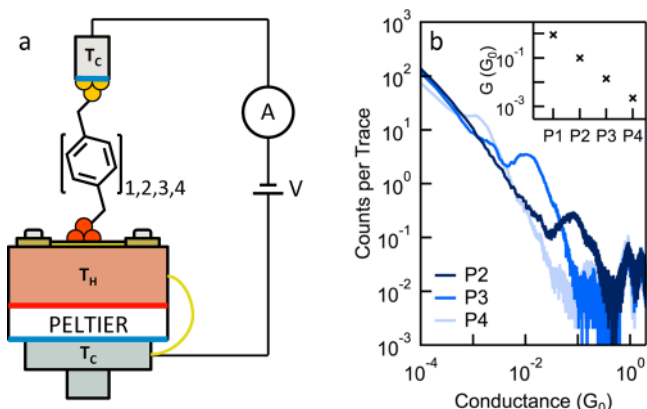

Figure 1. (a) Schematic of the STM-BJ setup representing thermoelectric measurement of **P1−P4**. (b) Conductance histograms of **P2−P4** obtained during the thermoelectric measurement. The bin size is 10^{-4} G_0. Inset: Conductance plotted as a function of number of phenyls in the molecular backbone.

formed between an Au STM tip and substrate by repeatedly bringing the substrate in and out of contact with the tip in an environment of the target molecules. The molecules used here are trimethylstannylmethyl-terminated oligophenyls with 1−4 phenyl rings (**P1−P4**) and trimethylstannyl[18] terminated alkanes (**C6**, **C8**, and **C10**) (see Supporting Information Figure S1 for structures), which were synthesized following

procedures detailed before.[12,19] These compounds are deposited onto the Au substrate from an acetone solution (~10 mM concentration). The trimethyl-tin (SnMe$_3$) terminations of the molecules cleave off in situ, yielding single-molecule junctions where the terminal carbon of the molecular backbone is covalently bonded to the Au electrode. The resulting junctions have a conductance that is significantly higher[12,19] than those formed with conventional linkers such as thiols,[16,20] amines,[17] or methyl sulfides.[21]

In these experiments, the molecular junction conductance is measured as a function of the relative tip/sample displacement yielding conductance traces. Conductance traces show plateaus at integer multiples of G_0, the quantum of conductance and typically an additional plateau at a molecule dependent conductance value. Thousands of conductance traces are collected for each compound and used to create one-dimensional conductance histograms. The linear-binned conductance histograms for **P2**, **P3**, and **P4** are given in Figure 1b with a bin size of 10^{-4} G_0. As the number of phenyls is increased, we see that the molecular junction conductance decreases exponentially as shown in the inset of Figure 1b. To confirm that these peaks are indeed due to the formation of an Au/molecule/Au junction, we also create two-dimensional conductance-displacement histograms. These are shown in Figure 2 for **P2−P4**. We see that the plateau length increases systematically as the molecular backbone length increases indicating that we are indeed measuring transport through these backbones.[22] The conductance feature between 10^{-5} and 10^{-4} G_0 in the case of **P2** in Figure 2a is due to the dimer molecule that forms in situ.[19] This dimer molecule has two biphenyls connected by a saturated 2-carbon bridge, giving it a much lower conductance than the fully conjugated **P4**. **P1** exhibits near resonant transport with a conductance of about 0.90 G_0.[19] Data for the alkanes is given in Supporting Information Figure S2 and reproduce our previous results well.[12]

Thermoelectric current and conductance across a single-molecule junction is measured simultaneously by applying a thermal gradient across the junction using a Peltier heater to controllably heat the substrate to temperatures ranging from room temperature to about 60 °C while maintaining the tip close to room temperature. The setup is allowed to come to thermal equilibrium for about one hour before measurements are carried out. In all measurements reported here, the temperature difference (ΔT) between the tip and substrate is set to either 0 or 14 K. Since we are probing the thermopower
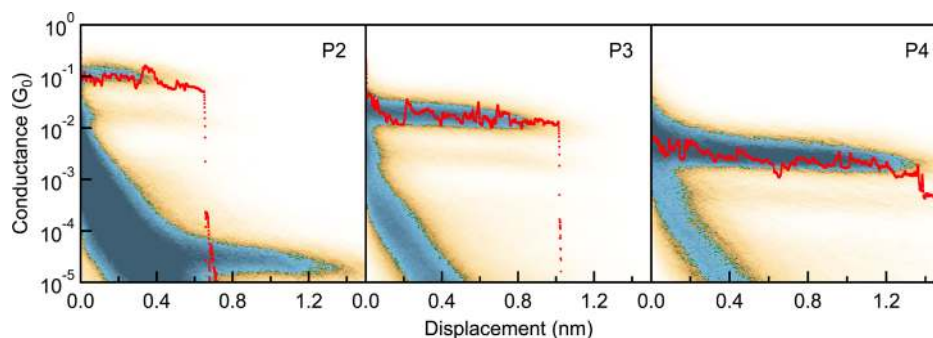

Figure 2. Two-dimensional conductance histograms of **P2−P4**. A representative conductance trace for each molecule is shown as a superimposed dotted lines. The bins have a width of 0.008 nm along the displacement axis and 100/decade along the conductance axis. The molecular plateau between 10^{-5} and 10^{-4} G_0 in the 2D histogram for **P2** is due to the dimer molecule formed in situ.

in the linear response regime (where the thermoelectric current increases linearly with the applied temperature difference), we do not need measurements at multiple temperatures. In order to minimize the impact of unaccounted thermoelectric voltages across the leads, a pure gold wire (99.998%) of known thermopower ($S_{Au} = 2$ μV/K) was connected from the hot side of the Peltier to the cold side (which was held near room temperature) to provide electrical connectivity and so that the thermoelectric voltage across the reverse temperature gradient ($-\Delta T$) was fixed (see Figure 1a for schematic). We measure the thermopower by setting the applied bias to 0 V and measuring the thermoelectric current through the circuit.

The thermopower measurement works as follows. The Au STM tip is brought into contact with the heated Au substrate while applying a bias voltage of 10 mV until a conductance greater than 5 G_0 is measured. The tip is then first retracted by 2.0 nm at a speed of ~16 nm/s, held fixed for 50 ms, and finally withdrawn an additional 1.6 nm. During part of the 50 ms hold section, we turn off the bias ($V = 0$) and continue to measure the current. We collect thousands of such current−displacement curves and select the ones that sustained a molecular junction through the entire "hold" portion of the ramp (see Supporting Information Figure S3).[23,8] We determine the average thermoelectric current for each such junction. The distributions of the average thermoelectric currents measured for **P2** are given in Figure 3a for $\Delta T = 0$ K (black, 386 traces),

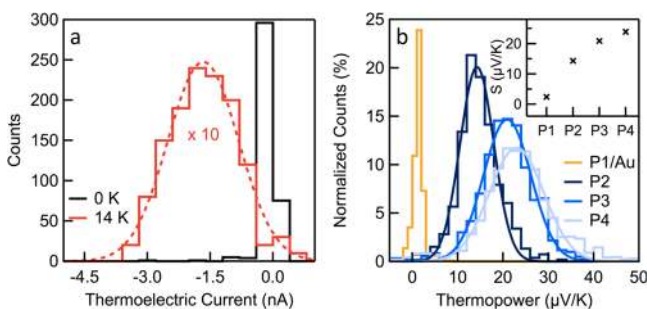**Figure 3.** (a) Average thermoelectric current histograms for **P2** for $\Delta T = 0$ K (black, 386 traces) and $\Delta T = 14$ K (red, 129 traces). The histogram at $\Delta T = 14$ K is multiplied by a factor of 10 for clarity and fit with a Gaussian (dotted line). (b) Histograms of thermopower for **P1/Au** (582 traces) and **P2** (530 traces), **P3** (629 traces), and **P4** (2942 traces). Gaussians fits to the histograms are also shown. Inset: Molecular thermopower plotted as a function of number of phenyls in the molecular backbone.

which is narrow and centered around 0 nA, and 14 K (red, 129 traces), which is broadened and peaked at −1.7 nA. Thermocurrent results from the other oligophenyl derivatives are given in Supporting Information Figure S4.

From the measured thermoelectric current, the thermopower of the single molecule junctions are calculated on a trace-by-trace basis ($S = I/G\Delta T$) and compiled into a histogram. The thermopower for all other molecules (**P1**, **P3**, **P4** and the three alkanes) were determined following the same procedure. Results from these measurements are given in Figure 3b for the oligophenyls and in Supporting Information Figure S5 for the alkanes. We have performed measurements of **P2** at a $\Delta T = 25$ K to verify that we are in the linear response regime (see Supporting Information Figure S6). We have also monitored the current during these measurements as a function of time to ensure that the temperature difference applied does not change

with time (see Supporting Information Figures S7). For **P1** (yellow curve in Figure 3b), we cannot distinguish, on a trace-by-trace basis, the difference between a molecular junction and a gold single-atom contact as the conductance of **P1** (0.9 G_0) is too close to that of the Au contact (1 G_0). We also see the thermopower for these junctions is very similar, that is, the distribution is peaked at 2.4 μV/K, indicating that the thermopower of an Au 1 G_0 junction is not very different from that of a **P1** junction. As the number of phenyl rings in the molecule is increased from 2 to 4, the center of the distributions of measured thermopower increases systematically. The values obtained for molecular conductance and thermopower using statistical fits to the data are given in Table 1 and are used to calculate the molecular power factor. We note

Table 1. Conductance, Thermopower, and Power Factor for All Molecules Measured

molecule	conductance (G_0)	thermopower (μV/K)	power factor (fW/K^2)
P1/Au	0.9	2.4	0.4
P2	1×10^{-1}	14.3	1.6
P3	1.4×10^{-2}	20.9	5×10^{-1}
P4	2×10^{-3}	23.9	9×10^{-2}
C6	1.4×10^{-2}	5.0	2.7×10^{-2}
C8	2×10^{-3}	5.6	5×10^{-3}
C10	3×10^{-4}	5.6	7×10^{-4}

that the power factor for **P2** (1.6fW/K^2) is higher than that of most other single molecule junction measurements with the exception of recent measurements with C60,[24] due to its high conductance and relatively high thermopower. Measurements for the alkanes are carried out in a similar way and all data are summarized in Table 1. We find that the thermopower of the alkanes does not have a strong dependence on the chain length from C6 to C10.

Our measurements show that the conductance of these oligophenyls decreases exponentially with increasing length, while the thermopower increases nonlinearly with increasing length. To rationalize these findings, we consider a series of models. In general, within the Landauer picture the zero-bias conductance is proportional to the electron transmission through the junction, evaluated at the electrode Fermi energy, E_F. In the simplest description of nonresonant transmission through a single molecule, a single frontier orbital controls the transmission. The transmission function can then be described by a Lorentzian function centered at the energy of that molecular level E_0 with a width, Γ, that relates to the electronic coupling of the molecular state to the electrodes. The exponential decrease in conductance as a function of molecule length must be captured by varying the model parameters.[7] We use our conductance and thermopower data for all the oligophenyls from the experiments to determine the corresponding single-Lorentzian transmission curves. Results are shown in Supporting Information Figure S8 where we see that we get unphysical parameters for E_0 and Γ. Specifically, the fit to experiment drives the backbone state to be pinned close to the Fermi energy, essentially independent of oligomer length.

To better understand trends in our conductance and thermopower data, we turn to tight-binding based model systems and calculate the conductances and thermopowers numerically using the Green's function approach[25−27] as detailed in the Supporting Information. We first consider a

simple improvement to the single-Lorentzian approximation discussed above that captures the length dependence explicitly. This tight-binding model (Model 1) assigns a single level to each phenyl ring and an electronic coupling (hopping parameter δ) between the rings. The terminal phenyls are coupled to the electrodes, as described by an imaginary self-energy $-i\Gamma/2$, (see Supporting Information Figure S9). The best fit-coefficients for the model are determined from experimental data as described in the Supporting Information. We find that this model tracks more closely the shift of the highest occupied molecular orbital toward the Fermi Energy yielding a transmission function where the resonances are fundamentally non-Lorentzian for all molecules with the exception of **P1** but predicts a strictly linearly increasing thermopower in contrast to what we see in the experiments.

For more insight to the electronic states in the junction, we examine results from calculations carried out using the density functional theory and non-equilibrium Green's functions (DFT-NEGF) formalism[28,29] with a gradient-corrected exchange-correlation functional.[30] The molecular junctions are described using a unit cell where each metallic layer consists of 16 atoms and the molecules are bound to gold mounds consisting of three atoms.[19] The junction geometry is first relaxed by minimizing the energy, allowing all molecular and tip atom degrees of freedom to move, and subsequent transport calculations are performed using the optimized structures. An exemplary **P4** junction structure is shown in Figure 4a. The DFT-calculated transmission spectra for **P1**−**P4** for an extended energy range are shown in Figure 4b. The narrow peaks positioned a few electron volts from the Fermi level correspond to the molecular backbone resonances. Low-bias conductance is however determined by the states representing the Au−C bonds. As visualized by the contour plot of the transmitted wave at the Fermi in Figure 4a, electrons enter the molecule through a gateway state (a σ Au−C bonding orbital) and then tunnel through the backbone, as evidenced by the decaying amplitude in the plot.

Returning to the transmission functions in Figure 4b, near the Au−C bond orbital resonances, the gateway states on opposite sides couple via this tunneling, resulting in a double-peak structure, where the deeper- (shallower-) energy peak is a bonding (antibonding) combination of the Au−C links.[12,19] For **P1**, the coupling is strong resulting in distinct features at −1.15 and −0.4 eV (**P1**), which merges into a single peak centered at $\sim$−0.6 eV for **P2**−**P4**. The tailing of these peaks to the Fermi level determines the low-bias conductance and thermopower of the **P1**−**P4** junctions. As shown in Figure 4d, the conductance calculated with DFT is overestimated due to the known errors within DFT that tend to place the key orbital energies in transport calculations too close to the electrode Fermi energy.[31−37] The thermopower, Figure 4e, is also overestimated and further the calculation does not show saturation with length. However, notice that while $G(E_F)$ is dramatically overestimated for **P2**−**P4**, the overestimation in the calculated values of S is smaller.

Overall, the key and robust feature that emerges from the DFT-based calculations is the role of the gateway state. The gateway states can introduce a qualitatively different trade-off between conductance and thermopower. The essential point is apparent in the transmission functions in Figure 4b where the amplitude of the peak near −0.6 eV drops approximately exponentially while the width remains approximately constant. To the extent that the width is constant, the thermopower will
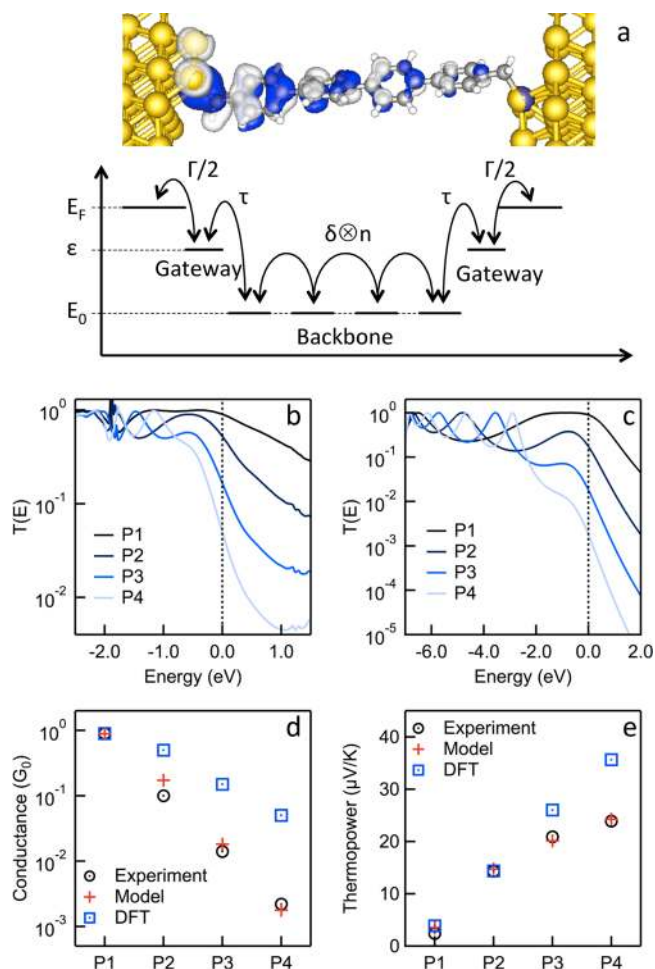

Figure 4. (a) Upper panel: The optimized geometry of a **P4** junction with an isosurface plot of the scattering state at the Fermi energy. Lower panel: Schematic diagram of the tight-binding model for **P4**. Transmission curves shown on a log scale for **P1**−**P4** (b) calculated using DFT and (c) as determined by the tight binding model using the best-fit parameters. (d) Conductance values and (e) thermopower determined form the experiment, tight-binding model, and DFT as a function of the number of phenyl units in the chain.

also be constant, being proportional to a normalized energy derivative of the transmission function. Motivated by the DFT results, we consider a second model that consists of two gateway states that are tunnel coupled to each other through a length dependent parameter $\delta_n = \delta_0 e^{-\beta n/2}$ ($n = 0$ is **P1**, etc.) These gateway states also interact with the electrodes through an imaginary energy independent self-energy term $-i\Gamma/2$. The parameter β describes the decay of transmission in the long-molecule limit and is assumed to be energy independent. More generally, from the complex band structure calculations in the polymeric limit,[38] we can expect an energy dependent $\beta(E)$ with a semielliptic shape spanning the energy gap between the occupied and empty frontier orbital derived bands that control tunneling. Details and results from fitting this model (Model 2) are shown in Supporting Information Figure S10. This model comes closer to describing the data but does not capture the exponential decay in conductance accurately as the value of β from the fit is found to be larger than what is measured in the experiment.[19] Furthermore, this model with an energy independent β yields a thermopower that saturates to

$$S_\infty = -\frac{\pi^2 k_B^2 T}{3e}\frac{\varepsilon}{4\varepsilon^2 + \Gamma^2}$$

in the long-molecule limit. As detailed in the Supporting Information, with an energy dependent β one would get an additional contribution to S proportional to oligomer length and $d\beta/dE$.

We improve on this by treating the backbone states explicitly while also including the gateway states in a tight-binding Hamiltonian as illustrated in Figure 4a. This combines the physical elements of models 1 and 2 and naturally incorporates $\beta(E)$ valid for energies near the occupied backbone states. The two gateway states at energy ε couple respectively to the left and right electrodes through the self-energy and they couple to a tight-binding chain that represents the essential frontier backbone orbitals with strength τ. The Hamiltonian for **P1** is a 3×3 matrix with no dependence on δ. The 4×4 matrix that represents the model Hamiltonian for **P2** is

$$H\{\mathbf{P2}\} = \begin{bmatrix} \varepsilon - i\Gamma/2 & \tau & 0 & 0 \\ \tau & E_0 & \delta & 0 \\ 0 & \delta & E_0 & \tau \\ 0 & 0 & \tau & \varepsilon - i\Gamma/2 \end{bmatrix}$$

The Hamiltonians for **P3** and **P4** can be obtained by extending this matrix. The best-fit model transmission curves are given in Figure 4c for all four using (in eV with $E_F = 0$) $\varepsilon = -1.85$, $\Gamma = 2.86$, $E_0 = -4.47$, $\tau = -2.28$, $\delta = -1.27$. The transmission curves are qualitatively very similar to the results from the DFT-based calculations. As seen in Figure 4d,e, the model gives a robust account of both the exponential drop in conductance and the partial saturation in the thermopower, which could not be seen in any of the other models or from the DFT based calculations.

DFT-based calculations for the alkanes are summarized in the Supporting Information Figure S11. The comparison to measured conductance and thermopower show the same trends as found for the **P1**–**P4** series. Furthermore, the transmission functions show the same key role for the Au–C gateway orbital. However, modeling the transmissions for these alkanes is not straightforward because the Fermi energy falls roughly halfway between the highest occupied and lowest unoccupied resonances.[38] Thus using just one molecular level for each methylene (as was done above with one level for each ring for the oligophenyls) does not capture the conductance trends correctly. Introducing an unoccupied level into our model will introduce more parameters than can be constrained by the limited data set available from the experiments and is thus beyond the scope of this work. Going back to the simpler model with two gateway states that are tunnel coupled to each other, we see that we would observe a nearly constant thermopower in the limit of large n when $d\beta/dE \approx 0$, as will be the case for alkanes when the Fermi energy falls near midgap.[38] We also note that measured thermopower for alkanes is sensitive to the link group. For example, it is much smaller in magnitude for phosphines[8] and negative for thiols.[7] A recent analysis of trends in thermopower in terphenyl with different link groups, based on DFT,[39,40] could be fruitfully extended to compare the role of the gateway state identified here for different linkers.

In summary, we have measured the conductance and thermoelectric properties of oligophenyls and alkanes bound to the electrodes through direct, covalent Au–C links. The highly conducting nature of these links gives rise to exceptional thermoelectric properties and high values of the power factor, GS^2, for the phenyl derivatives. A model for nanoscale transport in which only a frontier backbone orbital is considered, either through a single Lorentzian or by a tight-binding model that explicitly accounts for backbone length, does not correctly predict the observed dependences in conductance or thermo-power with length. Therefore, as motivated by the DFT calculations, we propose a modified tight-binding model to describe how transport is facilitated by a gateway Au–C state. This gateway-state is close in energy to the Fermi level and couples well into the molecular backbone, thereby dominating the zero-bias transmission properties of these molecules. For the alkanes, we find that conductance decreases exponentially while thermopower increases only modestly with the length of the molecule.

■ ASSOCIATED CONTENT

ⓢ Supporting Information
Additional information and figures. This material is available free of charge via the Internet at http://pubs.acs.org.

■ AUTHOR INFORMATION

Corresponding Author
*E-mail: (L.V.) lv2117@columbia.edu; (M.S.H.) mhyberts@ bnl.gov.

Notes
The authors declare no competing financial interest.

■ ACKNOWLEDGMENTS

■ REFERENCES

(1) Majumdar, A. *Science* **2004**, *303* (5659), 777−778.
(2) Snyder, G. J.; Toberer, E. S. *Nat. Mater.* **2008**, *7* (2), 105−114.
(3) Nitzan, A.; Ratner, M. A. *Science* **2003**, *300* (5624), 1384−1389.
(4) Kushvaha, S. S.; Hofbauer, W.; Loke, Y. C.; Singh, S. P.; O'Shea, S. J. *J. Appl. Phys.* **2011**, *109* (8), 084341−7.
(5) Tan, A.; Balachandran, J.; Dunietz, B. D.; Jang, S.-Y.; Gavini, V.; Reddy, P. *Appl. Phys. Lett.* **2012**, *101* (24), 243107−5.
(6) Tan, A.; Balachandran, J.; Sadat, S.; Gavini, V.; Dunietz, B. D.; Jang, S.-Y.; Reddy, P. *J. Am. Chem. Soc.* **2011**, *133* (23), 8838−8841.
(7) Malen, J. A.; Doak, P.; Baheti, K.; Tilley, T. D.; Segalman, R. A.; Majumdar, A. *Nano Lett.* **2009**, *9* (3), 1164−1169.
(8) Widawsky, J. R.; Darancet, P.; Neaton, J. B.; Venkataraman, L. *Nano Lett.* **2012**, *12* (1), 354−358.
(9) Baheti, K.; Malen, J. A.; Doak, P.; Reddy, P.; Jang, S. Y.; Tilley, T. D.; Majumdar, A.; Segalman, R. A. *Nano Lett.* **2008**, *8* (2), 715−719.
(10) Reddy, P.; Jang, S. Y.; Segalman, R. A.; Majumdar, A. *Science* **2007**, *315* (5818), 1568−1571.

(11) Malen, J. A.; Yee, S. K.; Majumdar, A.; Segalman, R. A. *Chem. Phys. Lett.* **2010**, *491* (4−6), 109−122.

(12) Cheng, Z. L.; Skouta, R.; Vazquez, H.; Widawsky, J. R.; Schneebeli, S.; Chen, W.; Hybertsen, M. S.; Breslow, R.; Venkataraman, L. *Nat. Nanotechnol.* **2011**, *6* (6), 353−357.

(13) Paulsson, M.; Datta, S. *Phys. Rev. B* **2003**, *67* (24), 241403.

(14) Dubi, Y.; Di Ventra, M. *Rev. Mod. Phys.* **2011**, *83* (1), 131−155.

(15) Ashcroft, N. W.; Mermin, N. D. *Solid State Physics*; Cengage Learning: Stamford, CT, 1976.

(16) Xu, B. Q.; Tao, N. J. *Science* **2003**, *301* (5637), 1221−1223.

(17) Venkataraman, L.; Klare, J. E.; Tam, I. W.; Nuckolls, C.; Hybertsen, M. S.; Steigerwald, M. L. *Nano Lett.* **2006**, *6* (3), 458−462.

(18) Khobragade, D.; Stensrud, E. S.; Mucha, M.; Smith, J. R.; Pohl, R.; Stibor, I.; Michl, J. *Langmuir* **2010**, *26* (11), 8483−8490.

(19) Chen, W.; Widawsky, J. R.; Vázquez, H.; Schneebeli, S. T.; Hybertsen, M. S.; Breslow, R.; Venkataraman, L. *J. Am. Chem. Soc.* **2011**, *133* (43), 17160−17163.

(20) Li, C.; Pobelov, I.; Wandlowski, T.; Bagrets, A.; Arnold, A.; Evers, F. *J. Am. Chem. Soc.* **2008**, *130* (1), 318−326.

(21) Park, Y. S.; Whalley, A. C.; Kamenetska, M.; Steigerwald, M. L.; Hybertsen, M. S.; Nuckolls, C.; Venkataraman, L. *J. Am. Chem. Soc.* **2007**, *129* (51), 15768−15769.

(22) Kamenetska, M.; Koentopp, M.; Whalley, A.; Park, Y. S.; Steigerwald, M.; Nuckolls, C.; Hybertsen, M.; Venkataraman, L. *Phys. Rev. Lett.* **2009**, *102* (12), 126803.

(23) Widawsky, J. R.; Kamenetska, M.; Klare, J.; Nuckolls, C.; Steigerwald, M. L.; Hybertsen, M. S.; Venkataraman, L. *Nanotechnology* **2009**, *43*, 434009.

(24) Evangeli, C.; Gillemot, K.; Leary, E.; González, M. T.; Rubio-Bollinger, G.; Lambert, C. J.; Agraït, N. *Nano Lett.* **2013**, *13* (5), 2141−2145.

(25) Nitzan, A. *Annu. Rev. Phys. Chem.* **2001**, *52*, 681−750.

(26) Hybertsen, M. S.; Venkataraman, L.; Klare, J. E.; Whalley, A. C.; Steigerwald, M. L.; Nuckolls, C. *J. Phys.: Condens. Matter* **2008**, *20* (37), 374115.

(27) Datta, S. *Electronic Transport in Mesoscopic Systems*; Cambridge University Press: New York, 1995.

(28) Soler, J. M.; Artacho, E.; Gale, J. D.; Garcia, A.; Junquera, J.; Ordejon, P.; Sanchez-Portal, D. *J. Phys.: Condens. Matter* **2002**, *14* (11), 2745−2779.

(29) Brandbyge, M.; Mozos, J. L.; Ordejon, P.; Taylor, J.; Stokbro, K. *Phys. Rev. B* **2002**, *65* (16), 165401.

(30) Perdew, J. P.; Burke, K.; Ernzerhof, M. *Phys. Rev. Lett.* **1996**, *77* (18), 3865−3868.

(31) Toher, C.; Filippetti, A.; Sanvito, S.; Burke, K. *Phys. Rev. Lett.* **2005**, *95* (14), 4.

(32) Evers, F.; Weigend, F.; Koentopp, M. *Phys. Rev. B* **2004**, *69* (23), 235411.

(33) Neaton, J. B.; Hybertsen, M. S.; Louie, S. G. *Phys. Rev. Lett.* **2006**, *97* (21), 216405.

(34) Ke, S. H.; Baranger, H. U.; Yang, W. T. *J. Chem. Phys.* **2007**, *126* (20), 201102.

(35) Sai, N.; Zwolak, M.; Vignale, G.; Di Ventra, M. *Phys. Rev. Lett.* **2005**, *94* (18), 186810.

(36) Thygesen, K. S.; Rubio, A. *Phys. Rev. B* **2008**, *77* (11), 115333.

(37) Thygesen, K. S.; Rubio, A. *Phys. Rev. Lett.* **2009**, *102* (4), 046802.

(38) Tomfohr, J. K.; Sankey, O. F. *Phys. Rev. B* **2002**, *65* (24), 245105.

(39) Balachandran, J.; Reddy, P.; Dunietz, B. D.; Gavini, V. *J. Phys. Chem. Lett.* **2012**, *3* (15), 1962−1967.

(40) Quek, S. Y.; Choi, H. J.; Louie, S. G.; Neaton, J. B. *ACS Nano* **2011**, *5* (1), 551−557.